Limnol. Oceanogr., 45(3), 2000, 628–641

Estimation of the absorption and backscattering coefficients from in-water radiometric measurements

Malgorzata Stramska[1]
Hancock Institute for Marine Studies, University of Southern California, Los Angeles, California 90089-0371

Dariusz Stramski
Marine Physical Laboratory, Scripps Institution of Oceanography, University of California, San Diego, La Jolla, California 92093-0238

B. Greg Mitchell
Marine Research Division, Scripps Institution of Oceanography, University of California, San Diego, La Jolla, California 92093-0218

Curtis D. Mobley
Sequoia Scientific, Inc., Westpark Technical Center, 15317 NE 90th Street, Redmond, Washington 98052

Abstract

Numerical simulations of radiative transfer within the ocean surface mixed layer have been used to derive a set of simple equations for estimating the absorption, a, and backscattering, b_b, coefficients in the blue-green spectral region from measurements of downwelling irradiance, E_d, upwelling irradiance, E_u, and upwelling nadir radiance, L_u. Two relationships are used in this derivation: (i) irradiance reflectance, $R = E_u/E_d$, is approximately proportional to b_b/a and inversely proportional to the average cosine of the underwater light field, μ; and (ii) radiance reflectance, $R_L = L_u/E_d$, is proportional to b_b/a but changes little with μ. Accordingly, μ is first estimated from L_u/E_u and then the absorption coefficient is obtained from Gershun's equation. Having determined a, b_b is estimated from the relation between R_L and b_b/a. We also show how the estimation of μ, a, and b_b is improved with additional data of the beam attenuation coefficient, c. The retrieval of a and b_b from E_d, E_u, and L_u has been tested using field data collected in the Southern California Bight. The a values predicted by the model show good agreement with absorption determinations from the ac-9 instrument and on-board spectrophotometric method, and the modeled b_b agrees well with the backscattering determinations from the Hydroscat-6 instrument. The algorithm has been derived for a broad range of the ocean inherent optical properties that do not necessarily covary with one another like in chlorophyll-based bio-optical models. However, the model should be used with caution if significant departure from the average Petzold particle scattering phase function is expected, for example in waters with high load of mineral particles.

The inherent optical properties (IOPs) of seawater are solely the properties of the medium and are fundamental to the understanding of the marine optical environment. The development of instrumentation for measuring IOPs and models for deriving the IOPs from the apparent optical properties (AOPs) have been essential to the objective of achieving accurate determinations of oceanic IOPs. Historically, accurate radiometric measurements of underwater light field allowing the calculations of AOPs have been more common and easier to achieve than measurements of IOPs. However, in recent years routine experimental work of optical oceanographers has been greatly enhanced by commercial availability of new instruments that allow determinations of IOPs from in situ measurements (Zaneveld et al. 1990; Moore et al. 1992; Maffione and Dana 1996). The ac-9 (WetLabs) and Hydroscat-6 (HobiLabs) instruments are now widely used for measuring the spectral absorption coefficient, $a(\lambda)$, and the backscattering coefficient, $b_b(\lambda)$, in the ocean.

With these technological advances, models that relate IOPs to AOPs can play a new role as a tool for estimating missing IOP data and for quality control of simultaneous measurements of IOPs and AOPs. This method of data quality control can be particularly useful for $a(\lambda)$ and $b_b(\lambda)$ because the present instruments used in these determinations do not provide direct measurements of these coefficients. The measurements of $a(\lambda)$ are subject to scattering errors that are difficult to estimate accurately. The Hydroscat-6 instrument measures light scattered at angles near 140°, and the conversion of the measured signal to $b_b(\lambda)$ involves un-

[1] Corresponding author.

Acknowledgments

This work was supported by NASA grant NAG5–6466 (M.S. and D.S.), NASA SIMBIOS grant NAS5–97130 (B.G.M.), and by the ONR Environmental Optics Program grants N00014-98-1-0003 (D.S.) and N00014-98-1-0247 (B.G.M.). Author C. M. acknowledges the ONR Environmental Optics Program, which supported in part the development of Hydrolight numerical model. Ship time was supported by the California Cooperative Fisheries Investigations (CalCoFI) cruises. We thank D. Kiefer for helpful discussions and anonymous reviewers for their comments.

certainty. Another role played by the models is that the determination of IOPs from light field measurements yields spatially averaged estimates for volumes of water that are large compared to small sampling volumes involved in the direct measurements of IOPs.

Our interest in this paper is in the particular class of models which enable one to determine IOPs from AOPs without any assumptions or a priori knowledge about the spectral behavior of IOPs. An approach to develop such models typically involves numerical simulations of underwater radiative transfer (e.g., Gordon et al. 1975; Kirk 1984, 1991; Gordon 1991). The vertical diffuse attenuation coefficient for downwelling irradiance, K_d, and the irradiance reflectance, $R = E_u/E_d$ (where E_d and E_u are the downwelling and upwelling plane irradiances respectively), were the AOPs used in these models. The model formulations involved K_d and R specified at the null depth just beneath the sea surface or at the midpoint of the euphotic zone. In addition, the estimation of IOPs, that is a and b_b or a and the total scattering coefficient b, required the knowledge of the surface conditions as model input or several measurements of AOPs throughout the day.

More recently, Gordon and Boynton (1997) presented an approach to derive $a(\lambda)$ and $b_b(\lambda)$, which is based on iterative simulations of radiative transfer. This method is computationally more intensive compared to previous models. In addition to measurements of depth profiles of the downwelling and upwelling irradiances, it requires guesses for the distribution of incoming radiance, sea state, and initial values of IOPs within the water column. Another recent model (Leathers and McCormick 1997) provides a method for determining a and b_b from depth profiles of E_d and E_u without the information about surface illumination and sea state. In this method the asymptotic values for K_d and R representing deep-water light regime are first estimated from irradiance measurements at arbitrary depths, and then a and b_b are determined from these asymptotic values. This approach is susceptible to less accurate results at shallow optical depths than at large depths.

In this paper we reexamine the radiative transfer simulations for a broad range of oceanic IOPs with the goal of deriving simple equations for estimating a and b_b from in-water measurements of E_d, E_u, and upwelling nadir radiance, L_u, under arbitrary and not necessarily known, sky conditions. We show that a and b_b at any depth z within the upper ocean can be estimated with simple equations that lead to reasonably small errors in the blue-green spectral region, even when the angular distribution of incoming solar radiation, sky conditions, and sea surface state are not known. Therefore, our model can be applied to data collected not only from ships but also from autonomous platforms such as moorings and drifters. We also show that the estimates of a and b_b can be improved if measurements of the beam attenuation coefficient are available in addition to E_d, E_u, and L_u. We compare the absorption estimates from the model with in situ measurements by the ac-9 instrument and onboard spectrophotometric analyses of water samples. The backscattering coefficients obtained from in situ measurements with the Hydroscat-6 instrument are also compared with the model retrieval.

Model description

Our model is based on extensive simulations of radiative transfer within the upper layers of the ocean, which allowed us to derive a set of equations for estimating the absorption and backscattering coefficients from in-water radiometric measurements of plane irradiances and upwelling radiance. Figure 1 schematically depicts the major steps involved in the development of the model, which is described in detail below.

Radiative transfer simulations—Simulations of the underwater light field were carried out with the Hydrolight radiative transfer numerical model based on the invariant imbedding theory (Mobley 1994). The model solves for the radiance averaged directionally in a number of directional bins defined by lines of constant polar (θ) and azimuthal (ϕ) angles, plus two polar caps. In our simulations the sphere was divided into 28 polar zonal bands of equal size and 36 azimuthal bands of equal size, plus two polar caps (total of 1,010 directional bins). The ocean was assumed to be infinitely deep and optically homogenous, i.e., with the scattering coefficient, absorption coefficient, and the scattering phase function constant with depth. The calculations were carried out down to a depth of 100–120 m. We assume that the results from these calculations can be applied to in situ data collected within the surface mixed layer, which is typically a few tens of meters.

The boundary conditions and the IOPs of water were modeled using the library of subroutines provided with the Hydrolight code. The surface boundary conditions included sky radiance distribution predicted for clear maritime atmosphere according to models of Gregg and Carder (1990), Harrison and Coombes (1988), and Kasten and Czeplak (1980). Although many simulations were run with the realistic sky radiance distribution and with a flat water surface, we also ran the model with a point sun in a black sky and with wind speeds of 5, 8, 10, and 15 m s^{-1} in order to check the sensitivity of our model to sea surface boundary conditions. The calculations were carried out for solar zenith angle of 0, 30, 60, and 80°. For each sun angle the calculations were repeated for various values of IOPs.

Two sets of input IOPs were used in radiative transfer simulations. The first set of IOPs simulated case 1 oceanic waters with chlorophyll *a* concentrations (*Chl*) ranging from 0.02 to 5 mg m^{-3}. This range represents most oceanic situations. The absorption and scattering coefficients were parameterized according to bio-optical models described in Gordon and Morel (1983) and Morel (1988; 1991). In the models of case 1 waters, all the IOPs covary with *Chl*. As a result, the IOPs also covary with one another. In order to relax this constraint and broaden the range of IOPs, we made another series of radiative transfer simulations. In these calculations, the set of input IOPs was specified in such a way that the IOPs changed independently of one another and covered a broad range of water turbidity (a up to ~1.5 m^{-1}, b_b up to ~0.022 m^{-1}, and ω_o from 0.3 to 0.85.

In all radiative transfer simulations the scattering phase function was parameterized as the sum of the contributions by pure water and particles. The particle component was

STEP 1
Specify two sets of input data for radiative transfer simulations:
Set I
sky radiance distributions for various solar angles
IOPs from bio-optical models parameterized in terms of *Chl* concentration
Set II
sky radiance distributions (same as above)
arbitrary a and b values which do not covary with one another

STEP 2
Simulate underwater light field with the Hydrolight radiative transfer model and estimate $\mu(z)$ (Eq. 3), $K_E(z)$ (Eq. 5), $R_L(z)=L_u(z)/E_d(z)$, $R(z)=L_u(z)/E_d(z)$, and $1/Q(z)=L_u(z)/E_u(z)$ for the specified input data.

STEP 3
Establish relationships between:
$R_L(z)$, $R(z)$ and $\mu(z)$
$b_b(z)$ and $a(z)$ $R_L(z)$

STEP 4
Derive estimates of :
$\mu(z)$ from Eqs. 7a and 7b
$a(z)$ from Eq. 8
$b_b(z)$ from Eqs. 9a and 9b

STEPS 5 – 7 only if the beam attenuation coefficient is known

STEP 5
Estimate $b(z)$ and $\omega_o(z)$ using Eqs. 11a - 11d

STEP 6
Derive improved estimates of $\mu(z)$ (Eq. 10)

STEP 7
Repeat calculations of $a(z)$ and $b_b(z)$ (Eqs. 8 and 9) using $\mu(z)$ from Step 6

Fig. 1. Summary of the steps involved in the development of our model.

taken as the average particle phase function from measurements made by Petzold (1972), as described in Mobley (1994). The backscattering ratio for this function is b_{bp}/b_p = 0.01811. We examined the sensitivity of the model to the assumption of a constant particle phase function. In these calculations we used particle phase functions estimated from Petzold's measurements in turbid waters of San Diego Harbor (b_{bp}/b_p = 0.01911), near-shore coastal waters in San Pedro Channel, California (b_{bp}/b_p = 0.0079), and clear ocean waters (b_{bp}/b_p = 0.01028).

Although our calculations were carried out for the spectrum of light from 350 to 700 nm with a 10-nm interval, the discussion presented below is focused on the spectral region from 400 to 560 nm, which is most important to ocean color

algorithms for determining phytoplankton pigments. The relationships derived in our model can be applied to any discrete wavelength within this region. All our radiative transfer simulations included Raman scattering. Fluorescence by dissolved organic matter was not simulated because it is rather poorly characterized and difficult to model with much confidence at the present time.

Conceptual background—A brief summary of the relationships between radiometric quantities, IOPs and AOPs is fundamental to our model development. The IOPs and AOPs are generally functions of light wavelength λ and depth z, but for simplicity we will omit λ and z from notation unless specifically required. The irradiance reflectance is a ratio of upwelling to downwelling irradiance ($R = E_u/E_d$). Because of interest in remote sensing of ocean color, much effort in the past focused on reflectance just beneath the water surface, $R(z = 0^-)$. The main result is that such reflectance is approximately proportional to the ratio of the backscattering coefficient to the absorption coefficient for waters with low to moderate turbidity, that is when $b_b \ll a$ (Morel and Prieur 1977; Kirk 1984; Gordon and Morel 1983):

$$R(z = 0^-) = f\, b_b/a \tag{1}$$

The factor f is not constant and it depends primarily on the angular structure of the light field incident on the sea surface and the volume scattering function of seawater (Kirk 1991; Morel and Gentili 1991; 1993). Specifically, f increases nearly linearly with a decrease in μ_o, the cosine of the zenith angle of the refracted direct solar beam just beneath the sea surface. As a result, $R(z = 0^-)$ can increase by tens of percentage when the solar zenith angle changes from 0 to 80°. The inverse relation between the irradiance reflectance and the average cosine of light field at great depths in turbid water has also been studied (Timofeeva 1979).

Alternatively, instead of irradiance reflectance R, one can use the radiance reflectance R_L defined as the ratio of the upwelling nadir radiance (L_u) to downwelling irradiance (E_d). In analogy to Eq. 1, $R_L(z = 0^-)$ just beneath the sea surface can be related to the IOPs:

$$R_L(z = 0^-) = (f/Q)(b_b/a) \tag{2}$$

where Q ($= E_u/L_u$) is the ratio of the upwelling irradiance to the upwelling radiance (Morel and Gentili 1993). Based on Monte Carlo simulations, Morel and Gentili provided a detailed discussion of variations in the Q factor with geometrical variables (direction of radiance and solar zenith angle) and the IOPs of seawater. They also pointed out that the factors f and Q covary with changes in the Sun's position in such a way that the ratio f/Q is less sensitive to the angular distribution of the light than each of the factors considered separately.

If we assume that $R(z)$, i.e., the reflectance at depth z, is proportional to $b_b(z)/a(z)$ and inversely proportional to the average cosine of the light field at that particular depth, $\mu(z)$, and that $R_L(z)$ is approximately proportional to $b_b(z)/a(z)$ but is not very sensitive to the directional structure of the light field, then we can estimate $\mu(z)$ from the ratio of $R_L(z)/R(z) = L_u(z)/E_u(z)$. An algorithm for estimating $a(z)$ and $b_b(z)$ from radiometric measurements that we will derive below is based on this assumption. Accordingly, the average cosine $\mu(z)$ defined as

$$\mu(z) = [E_d(z) - E_u(z)]/E_o(z) \tag{3}$$

where $E_o(z)$ is the scalar irradiance, is first estimated from $R_L(z)$ and $R(z)$ using a relationship derived from the radiative transfer simulations. The Gershun law is then used to estimate $a(z)$:

$$a(z) = K_E(z)\mu(z) \tag{4}$$

where the vertical attenuation for net irradiance, $K_E(z)$, is obtained from measurements of $E_d(z)$ and $E_u(z)$:

$$K_E(z) = -\mathrm{d}\,\ln[E_d(z) - E_u(z)]/\mathrm{d}z \tag{5}$$

Finally, the backscattering coefficient, $b_b(z)$, is estimated from Eq. 2 using the relationship between $R_L(z)$, $b_b(z)$, and $a(z)$, which is again obtained through radiative transfer simulations:

$$b_b(z) \sim a(z)R_L(z) = a(z)L_u(z)/E_d(z) \tag{6}$$

Equation 4 assumes that inelastic scatter and internal light sources are negligible. We discuss the limitations of this assumption below.

Results from the radiative transfer simulations—The values of K_E, R, and R_L calculated by Hydrolight simulations at several water depths between 1 and 80 m as a function of the input a and b_b coefficients are displayed in Fig. 2. In general, for a given set of IOPs, the AOPs vary with the angular distribution of light, and therefore with water depth and solar zenith angle. Figure 2 illustrates how significant these effects are for each of the discussed AOPs. First, K_E varies by more than 30% for a given absorption coefficient (Fig. 2A). Second, there is also a large scatter of data points in the R versus b_b/a relationship. For the same value of b_b/a, R can vary by more than 50% (Fig. 2C). The data points are less scattered if we plot the product of R and μ versus b_b/a (Fig. 2D). Finally, R_L is better approximated by a linear function of b_b/a (Fig. 2B) than R, which indicates that R_L is less dependent on the angular distribution of light. This observation is consistent with the modeling results for the reflectance just beneath the water surface (Morel and Gentili 1993) and with recent experimental data, which showed that R_L in the blue-green spectral region measured at 15-m depth in clear ocean waters changed little in response to variable solar altitude (Stramska and Frye 1997).

Raman scattering can lead to a significant departure from the classical Gershun law presented in Eq. 4. Our radiative transfer calculations indicate that in the top 20 m of the water column this departure is not significant for wavelengths less than 560 nm, and the product of K_E and μ differs from the absorption coefficient by 2% in the worst case ($\lambda = 560$ nm and $Chl = 0.02$ mg m^{-3}). Therefore, Raman scattering will not significantly affect our estimates of a at these depths. Another effect of Raman scattering is to increase reflectances compared to what would be observed without Raman scattering. In general, the influence of Raman scattering on the reflectances in the spectral range 500–560 nm increases with increasing λ and z (Stavn 1993), and decreasing Chl. Our simulations indicate that for $Chl = 0.05$ mg

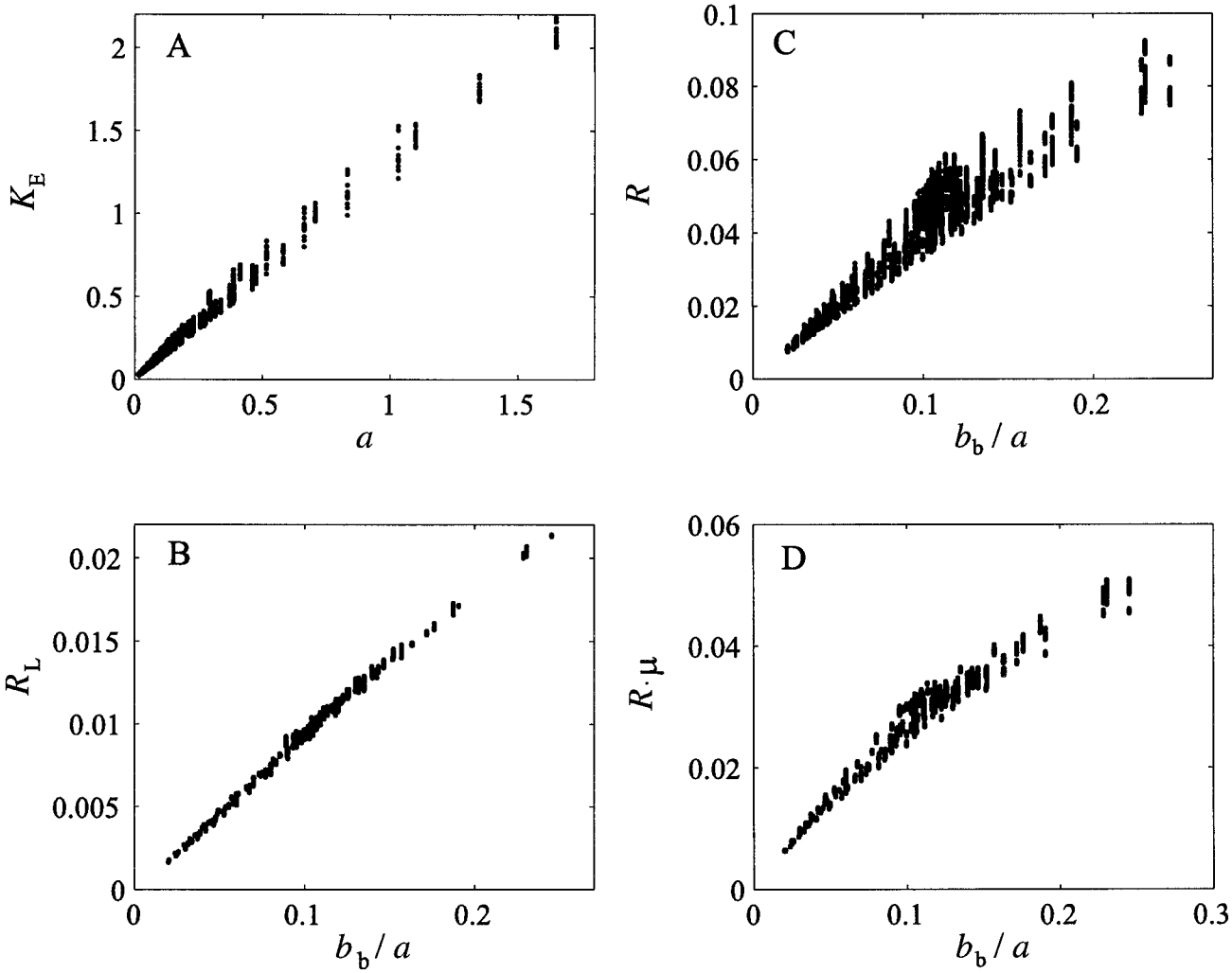

Fig. 2. Results of the radiative transfer simulations showing the relationships between the various AOPs and IOPs. (A) The vertical attenuation coefficient for net irradiance, K_E (m^{-1}), as a function of absorption coefficient, a (m^{-1}). (B) The relationship between the radiance reflectance, $R_L = L_u/E_d$, and the ratio of the backscattering coefficient to the absorption coefficient, b_b/a. (C) The relationship between the irradiance reflectance, $R = E_u/E_d$, and the ratio of the backscattering coefficient to the absorption coefficient, b_b/a. (D) The relationship between the product of E_u/E_d and μ, and the ratio b_b/a. In the simulations we assumed cloudless maritime sky and a flat sea surface. The data were obtained for the zenith sun angles of 0, 30, 60, and 80°, and wavelengths from 400 to 560 nm with 10-nm intervals.

m^{-3}, $R_L(510)$ at $z = 15$ m with Raman scattering is higher by 17% than without Raman scattering. The R_L value at 560 nm for the same water depth and *Chl* is higher by 30%. At a 5-m depth this effect for 560 nm decreases to about 15%. Similar effects are observed for the irradiance reflectance. Importantly, because our estimates of μ are based on the ratio of R_L/R, the effect of Raman scattering nearly cancels out in the estimation of μ. However, our estimate of b_b is proportional to R_L, therefore we expect that the errors in the derived b_b will increase with increasing water depth and decreasing *Chl*. Accordingly, our results for the spectral range of 500–560 nm will be limited to the top 15 meters of the water column, unless otherwise indicated.

First approximation of μ, a, and b_b—In deriving our algorithm for estimating μ, a, and b_b, we assume that the values of E_d, E_u, L_u, and c are available from measurements. However, the first approximation estimates of μ, a, and b_b require only measurements of E_d, E_u, and L_u. The beam attenuation coefficient c is required for the improved algorithm described in the next section.

Based on the data set generated by radiative transfer simulations with the average Petzold particle phase function and a range of water turbidity with $c \leq 2$ m^{-1}, the average cosine μ for any blue wavelength from the spectral range 400–490 nm, denoted as λ_b, can be estimated from

$$\mu_{est}(\lambda_b) = [-37.8266 R_L^2(\lambda_b) + 2.3338 R_L(\lambda_b) + 0.00056]/R(\lambda_b) + 0.1993 \quad (7a)$$

where the subscript ''est'' is used to indicate the estimated value. Upon comparing μ_{est} with true values of μ, obtained directly from radiative transfer calculations through Eq. 3, we find that the maximum error of the retrieval of μ in the

blue is less than 13% (Fig. 3). For green wavelengths λ_g from the spectral range 500–560 nm the following relationship has been obtained

$$\mu_{est}(\lambda_g) = [-28.88966R_L{}^2(\lambda_g) + 3.248438R_L(\lambda_g) - 0.001400]/R(\lambda_g) + 0.080558 \quad (7b)$$

The maximum error of the retrieval of μ for λ_g is about 12% (Fig. 4). Next, we estimate the absorption coefficient by substituting μ_{est} for μ in Eq. 4:

$$a_{est}(\lambda_b \text{ or } \lambda_g) = K_E(\lambda_b \text{ or } \lambda_g)\mu_{est}(\lambda_b \text{ or } \lambda_g) \quad (8)$$

The relationships for the backscattering coefficient are

$$b_{b,est}(\lambda_b) = 11.3335R_L(\lambda_b)a(\lambda_b) - 0.0002 \quad (9a)$$

$$b_{b,est}(\lambda_g) = 10.8764R_L(\lambda_g)a(\lambda_g) - 0.0003 \quad (9b)$$

where the $b_{b,est}$ values are calculated by substituting $a(\lambda_b)$ and $a(\lambda_g)$ with a_{est} at appropriate wavelengths. The estimated absorption and backscattering coefficients are plotted against true values of these coefficients (i.e., input to Hydrolight simulations) in Figs. 3, 4. For $Chl < 5$ mg m^{-3}, the maximum error of the retrieval of a and b_b for the blue wavelengths is less than 12%. Maximum error for a in the green spectral region is also less than 12%, but error of the b_b retrieval can be higher. For example, at the 15-m depth and $Chl = 0.02$ mg m^{-3} this error reached 29% and 30% for 510 and 560 nm, respectively. However, if $Chl > 0.1$ mg m^{-3}, this error was always less than 12% and 20% for the 500–530 and 540–560 nm bands, respectively.

Improved estimation of μ, a, and b_b—The above analysis suggests that the retrieval of a and b_b would improve with more accurate estimation of μ. Therefore, we will now examine the relationship between μ and reflectances in greater detail. Our data indicate that for a given set of IOPs, μ can be accurately estimated from the ratio $R_L/R = L_u/E_u$. Five examples from our radiative transfer simulations showing a dependence of μ on L_u/E_u are plotted in Fig. 5A. Each example corresponds to one specified set of IOPs. In each case the data points follow a linear relationship between μ and L_u/E_u. The variation in μ and L_u/E_u along these lines is associated with the fact that the data points correspond to various depths and solar angles. Importantly, each ''family of points'' is shifted along the L_u/E_u axis because of changes in the IOPs. This shift is responsible for a relatively large dispersion of the data points observed earlier in Figs. 3, 4. Thus, to improve the estimates of μ we will in this section develop a parameterization of the shifts between various groups of data points in terms of variations in the IOPs. Before doing this, we note that the relationship between μ and L_u/E_u appears to be insensitive to changes in the angular distribution of light reaching the sea surface or sea surface conditions. This is shown in Figs. 5B, 5C where we combine

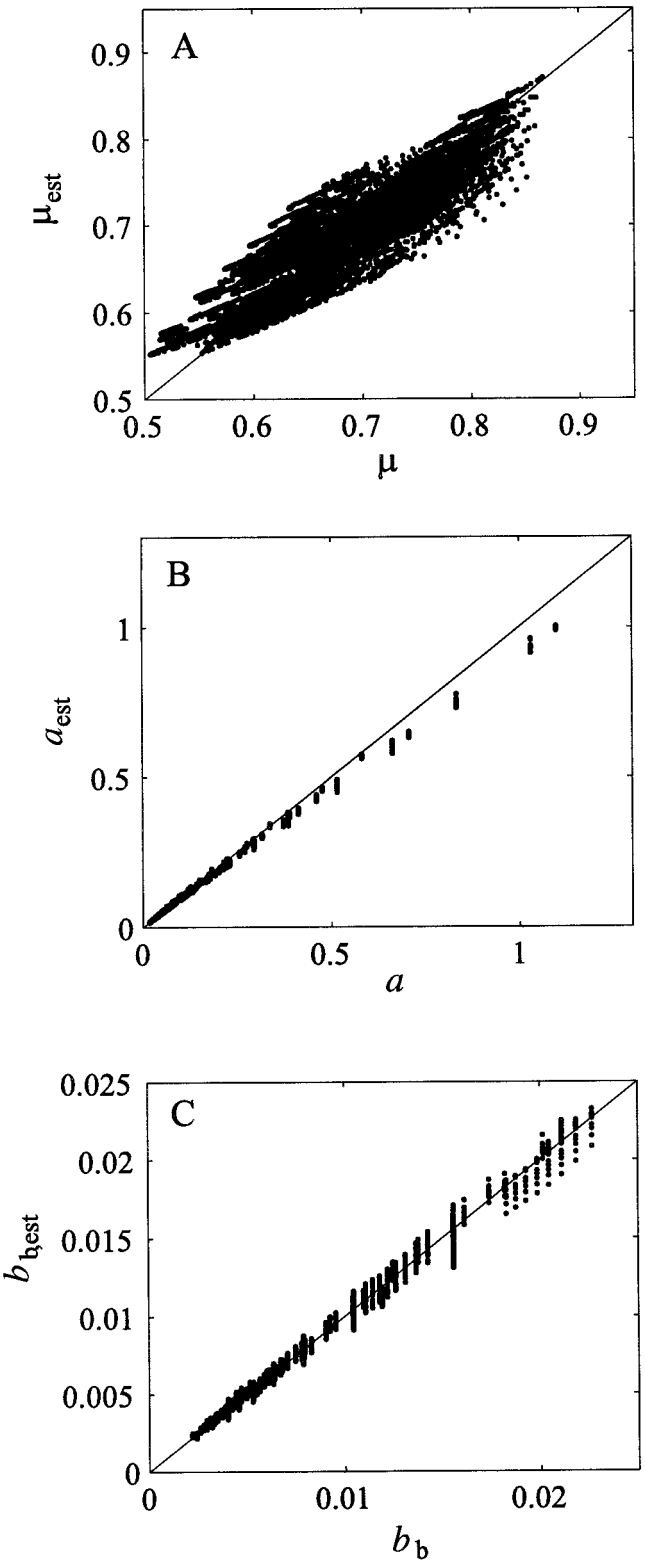

Fig. 3. Results of the radiative transfer simulations for the 400–490 nm spectral region. (A) The relationship between the true average cosine of the light field, μ, and the average cosine μ_{est} estimated from Eq. 7a. The squared correlation coefficient r^2 is 0.89. (B) The relationship between the true absorption coefficient, a (m^{-1}), and the absorption coefficient, a_{est} (m^{-1}), estimated using Eq. 8; r^2 is 0.99. (C) The relationship between the true backscattering coefficient, b_b (m^{-1}) and the backscattering coefficient, $b_{b,est}$ (m^{-1}) estimated from Eq. 9a; r^2 is 0.99.

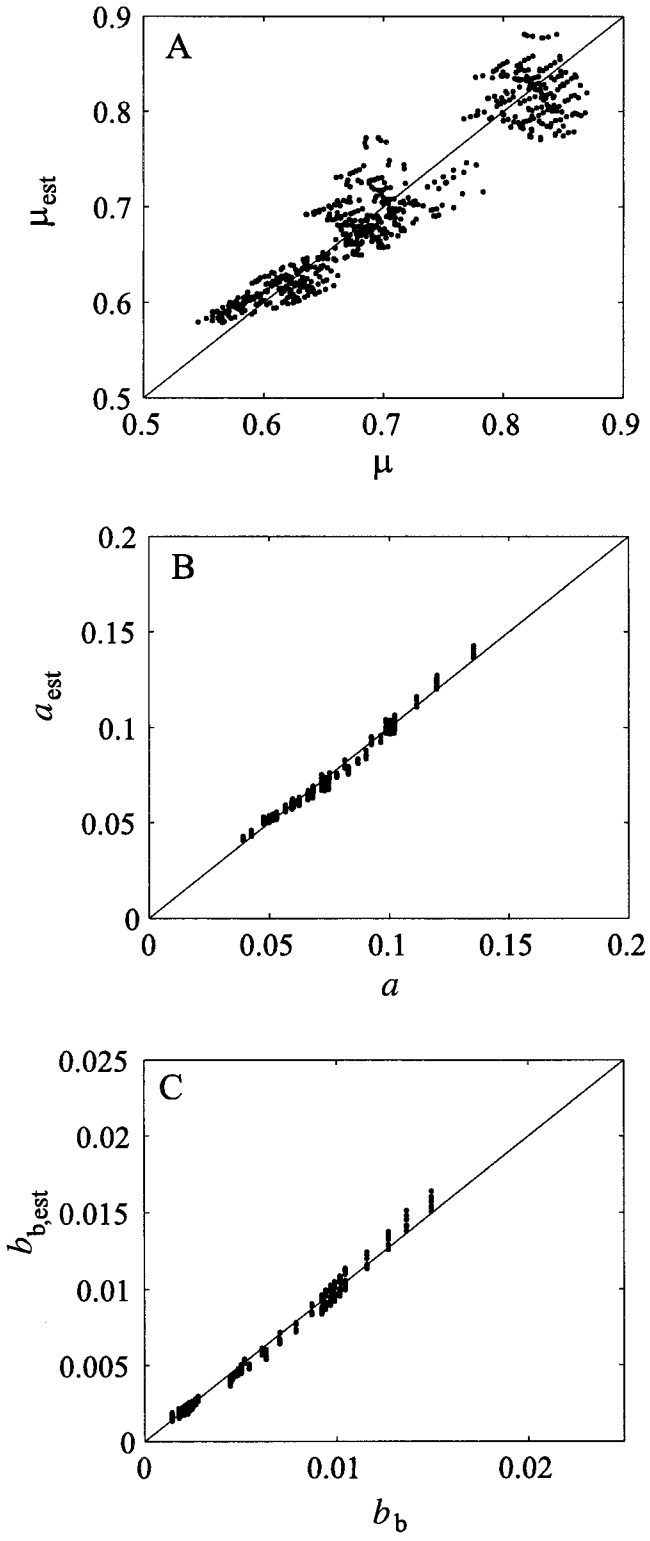

Fig. 4. As Fig. 3, but the data points shown are for the 500–560 nm spectral region. The coefficient r^2 is 0.96, 0.99, and 0.99 for data shown in Figs. 4A, 4B, and 4C, respectively.

the results of model simulations for the point sun located in the black sky and wind speed of 0 and 8 m s^{-1}, and for the realistic sky and wind speed of 0, 5, and 15 m s^{-1}.

The IOPs governing the radiative transfer are the single-scattering albedo, $\omega_o = b/c$, and the volume scattering function (VSF), which in our model is the sum of the pure water contribution and the forward-peaked function for particles. Thus, the overall shape of VSF varies due to the changes in the relative proportions of molecular scattering and particle scattering when *Chl* is changing. Changes in the shape of VSF also occur throughout the light spectrum because the contribution of molecular scattering is wavelength dependent. The relative importance of the molecular water and particulate scattering can be parameterized by the ratio of the backscattering coefficient to the total scattering coefficient, b_b/b. Therefore we will describe the relationship between μ and L_u/E_u in terms of its dependence on b_b/b and ω_o.

The results are based on the radiative transfer simulations made for the b_b/b ratio varying from 0.025 to 0.07. For each value of the b_b/b, a sequence of calculations was carried out for a set of ω_o values. Next, for each of these simulations, a linear regression for μ versus L_u/E_u was determined. The values for intercept and slope of these regressions are plotted in Fig. 6 as a function of ω_o and b_b/b. The results indicate that the linear regression of μ versus L_u/E_u depends on both b_b/b and ω_o in a fairly regular manner. Therefore, the parameterization of μ versus L_u/E_u in terms of ω_o and b_b/b is possible (Table 1).

Using equations given in Table 1, improved estimates of μ can be derived from

$$\mu_{est2} = \text{slope } L_u/E_u + \text{intercept} \tag{10}$$

where the slope and intercept parameters depend on ω_o and b_b/b. The scattering coefficient b can be approximated in two ways. First, b can be obtained from the measured beam attenuation coefficient c and the first estimate of absorption a_{est}:

$$b_1 = c - a_{est} \tag{11a}$$

Second, assuming that the backscattering probability for particles is 0.01811 (in agreement with the average Petzold function), b can be obtained from $b_{b,est}$ using the pure seawater scattering coefficient b_w taken from Morel (1974):

$$b_2 = b_w + [b_{b,est} - 0.5\ b_w]/0.01811 \tag{11b}$$

If a_{est} is an overestimate, then b_1 is an underestimate and b_2 is an overestimate of true b. The opposite is the case if a_{est} is underestimating true absorption. Therefore, we estimate b as

$$b_{est} = (b_1 + b_2)/2 \tag{11c}$$

and then we obtain an estimate of ω_o according to

$$\omega_{o,est} = b_{est}/c \tag{11d}$$

Using the calculated $b_{b,est}/b_{est}$ and $\omega_{o,est}$, we then interpolate between the formulas displayed in Table 1 to obtain the slope and intercept of Eq. 10. As a final step, after calculating μ_{est2} for a given measured value of L_u/E_u, we substitute μ_{est2} in place of μ_{est} in Eq. 8 to obtain an improved estimate of

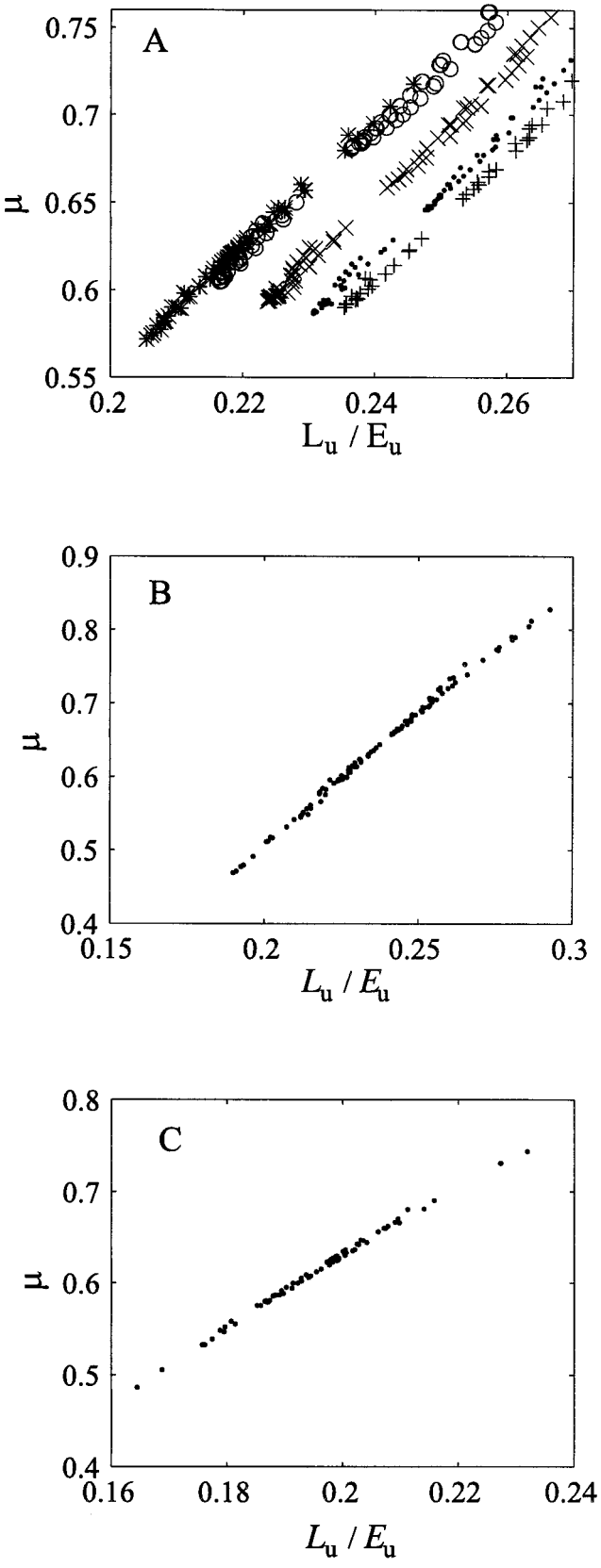

Fig. 5. Examples of the relationship between the average cosine μ and L_u/E_u. (A) Simulations for cloudless maritime sky and a flat sea surface. Data indicated by large crosses are for 415 nm and *Chl* = 0.075 mg m^{-3}; dots for 415 nm and *Chl* = 0.1 mg m^{-3}; small crosses for 445 nm and *Chl* = 0.1 mg m^{-3}; circles for 485 nm and *Chl* = 0.075 mg m^{-3}; and stars for 415 nm and *Chl* = 0.5 mg m^{-3}. (B) Data obtained for 445 nm and *Chl* = 0.1 mg m^{-3} and for five sets of boundary conditions: point sun located in the black sky with a wind speed of 0 and 8 m s^{-1}, and cloudless maritime sky with a wind speed of 0, 5, and 15 m s^{-1}. (C) Data points obtained for 445 nm, *Chl* = 2 mg m^{-3}, and for five sets of boundary conditions: point sun located in the black sky with a wind speed of 0 and 8 m s^{-1}, and cloudless maritime sky with a wind speed of 0, 5, and 15 m s^{-1}.

absorption, and we then calculate the backscattering coefficient from Eq. 9a or 9b using this improved estimate of absorption.

The results of the calculations of improved estimates of μ, a, and b_b for our data set generated with the radiative transfer simulations are shown in Fig. 7. The errors of retrieval of μ, a, and b_b decreased compared to the first approximation. For example, for the blue spectral region 400–490 nm and *Chl* $<$ 5 mg m^{-3}, the errors are now always less than 5% and the average error is less than 1% for each of the estimated quantities. These errors are for a flat sea surface, but our additional calculations indicated that the maximum errors would increase by less than 1% if the data for wind speed of 5, 8, and 15 m s^{-1} were included in the analysis. In the spectral range 500–560 nm, the maximum error of μ and a estimates is less than 10%. However, the error in the b_b retrieval for *Chl* = 0.02 mg m^{-3} is as high as for the first approximation estimates. For *Chl* $>$ 0.05 mg m^{-3} this error within the upper 10-m water column does not exceed 12% and 15% for 500–530 and 540–560 nm, respectively. For *Chl* $\geq$ 0.1 mg m^{-3} and 10-m water depth the maximum errors in estimates of μ, a, and b_b in the green spectral region are less than 5%, 5%, and 12%, respectively.

Our relationships were developed using simulations for optically homogenous water. Additional calculations indicate that the approach works reasonably well when the water column is inhomogeneous. This is shown in Figs. 8, 9 where the results from two model simulations of nonuniform vertical chlorophyll distributions are presented. The estimates of μ, a, and b_b from the model are virtually indistinguishable from the true values in the top portion of the water column and a small discrepancy is observed only at water depths with strong gradients of IOPs. The maximum error of these estimates is about 7%.

Sensitivity to particle phase function—In order to examine the sensitivity of our model to the particle phase function, we applied the above relationships derived for the average particle phase function (b_{bp}/b_p = 0.01811) to the results from radiative transfer simulations with Petzold's particle phase functions for turbid waters of San Diego Harbor (b_{bp}/b_p = 0.01911), clear ocean waters (b_{bp}/b_p = 0.01026), and nearshore coastal waters in the San Pedro Channel (b_{bp}/b_p = 0.00790). When the model based on the average particle phase function was applied to the data representing the San Diego Harbor phase function, the errors in the estimated μ

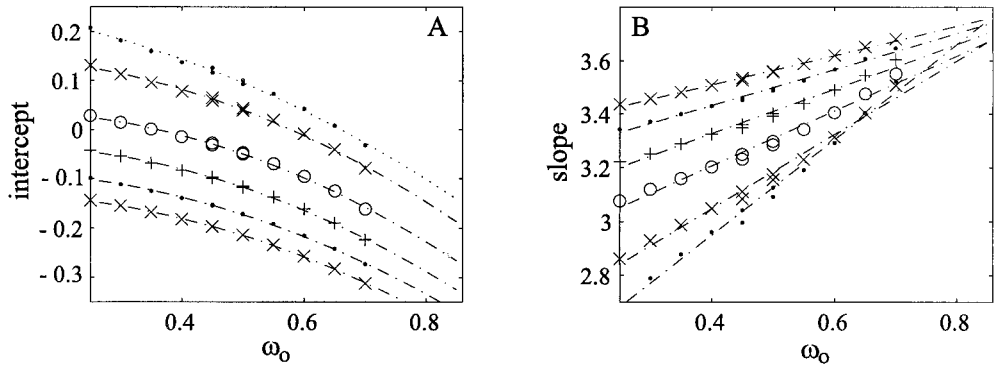

Fig. 6. Results of the radiative transfer simulations: (A) The dependence of the intercept of the relationship between μ and L_u/E_u on ω_o with b_b/b as a parameter. The curves from the top (dotted line) to bottom (crosses and dash-dot line) are for b_b/b of 0.025, 0.03, 0.04, 0.05, 0.06, and 0.07, respectively. Each curve has been approximated as a second order polynomial (*see Table 1*). (B) The dependence of the slope of the relationship between μ and L_u/E_u on ω_o with b_b/b as a parameter. The curves from the bottom to top in the left-hand side of the plot correspond to b_b/b of 0.025, 0.03, 0.04, 0.05, 0.06, and 0.07, respectively. Linear equations describing each set of points are given in Table 1.

and a were below 5%, and the errors in b_b were less than 14%. However, in the case of the San Pedro Channel phase function, the maximum errors for μ and a increased to 15% and for b_b to 40%. Considering these effects, the algorithm derived for the average particle phase function should be applied with caution when significant deviations from this function are expected. Our tests showed that in such a case, a refined algorithm accounting for variability of particle phase function can reduce errors. Specifically, when we used our model with new coefficients derived from simulations including all four Petzold particle phase functions, the maximum error for the retrieval of μ and a decreased to 11% and for b_b to 20%. Clearly, there is a need to further investigate the variability of the phase function in the ocean. With the progress in this area our algorithm can be refined to minimize errors that result from this variability.

Comparison of the model with field measurements

We compared the first-approximation estimates of a and b_b obtained from our model with the corresponding data from field measurements collected during three California Cooperative Oceanic Fisheries Investigations (CalCoFI) cruises in the Southern California Bight. Two cruises (June and September 1998) provided data of all radiometric quantities necessary to use our model, that is $E_d(\lambda)$, $E_u(\lambda)$, $L_u(\lambda)$, and both IOPs that are retrieved with the model, that is $a(\lambda)$ and $b_b(\lambda)$. For the third cruise (April 1998), all the data with the exception of $b_b(\lambda)$ are available. The data were collected at different times of the day under various conditions including clear, partly cloudy, and overcast skies, as well as variable sea states, which ensures variation in the angular distribution of incoming light.

Table 1. Polynomial functions fitted by the least squares method to the data points shown in Fig. 6A, B.

b_b/b	Intercept	Slope
0.025	$-0.4175\ \omega_o^2 - 0.1115\ \omega_o + 0.2553$	$1.7762\ \omega_o + 2.2381$
0.03	$-0.4997\ \omega_o^2 + 0.0275\ \omega_o + 0.1510$	$1.3793\ \omega_o + 2.4954$
0.04	$-0.5309\ \omega_o^2 + 0.0991\ \omega_o + 0.0333$	$1.0286\ \omega_o + 2.7946$
0.05	$-0.5105\ \omega_o^2 + 0.0955\ \omega_o - 0.0373$	$0.8350\ \omega_o + 2.9924$
0.06	$-0.4602\ \omega_o^2 + 0.0617\ \omega_o - 0.0882$	$0.6745\ \omega_o + 3.1622$
0.07	$-0.4450\ \omega_o^2 + 0.0560\ \omega_o - 0.1315$	$0.5482\ \omega_o + 3.2903$

Methods consistent with the SeaWiFS protocols were used to collect the data (Mueller and Austin 1992). The underwater vertical profiles of downwelling and upwelling irradiances, $E_d(z, \lambda)$ and $E_u(z, \lambda)$, and upwelling radiance, $L_u(z, \lambda)$, were measured with a MER-2048 spectroradiometer (Biospherical Instruments). The backscattering coefficient, $b_b(z, \lambda)$, was determined from measurements with a Hydroscat-6 sensor (HobiLabs). The vertical profiles of spectral absorption, $a(z, \lambda)$, and beam attenuation, $c(z, \lambda)$, were measured with an ac-9 meter (WetLabs). The Hydroscat-6 and ac-9 instruments were interfaced with MER-2048 into one system, which also included CTD probe (SeaBird), single-wavelength beam transmissometer and fluorometer (Sea-Tech). In addition, the absorption spectra by particulate and soluble materials were measured on water samples taken from discrete depths with the ship's CTD-rosette, using an on-board double-beam spectrophotometer. The particulate absorption spectra $a_p(z, \lambda)$ were determined with a filter-pad technique (Mitchell 1990). The absorption by soluble organic matter, $a_s(z, \lambda)$, was measured in 10-cm quartz cuvettes on samples filtered through a pre-rinsed 0.2 μm Nuclepore filter, relative to Milli-Q water (Bricaud et al. 1981). Water samples were usually taken shortly before or after the optical casts, but occasionally these events were separated by more than 1 hour. The methods and data processing procedures applied to CalCoFI data are described in greater detail in Mitchell and Kahru (1998).

For comparison of the model estimates and field observations, we will use data from the blue spectral region. Although the wavelengths sampled by various instruments did not exactly match each other, the differences in the blue

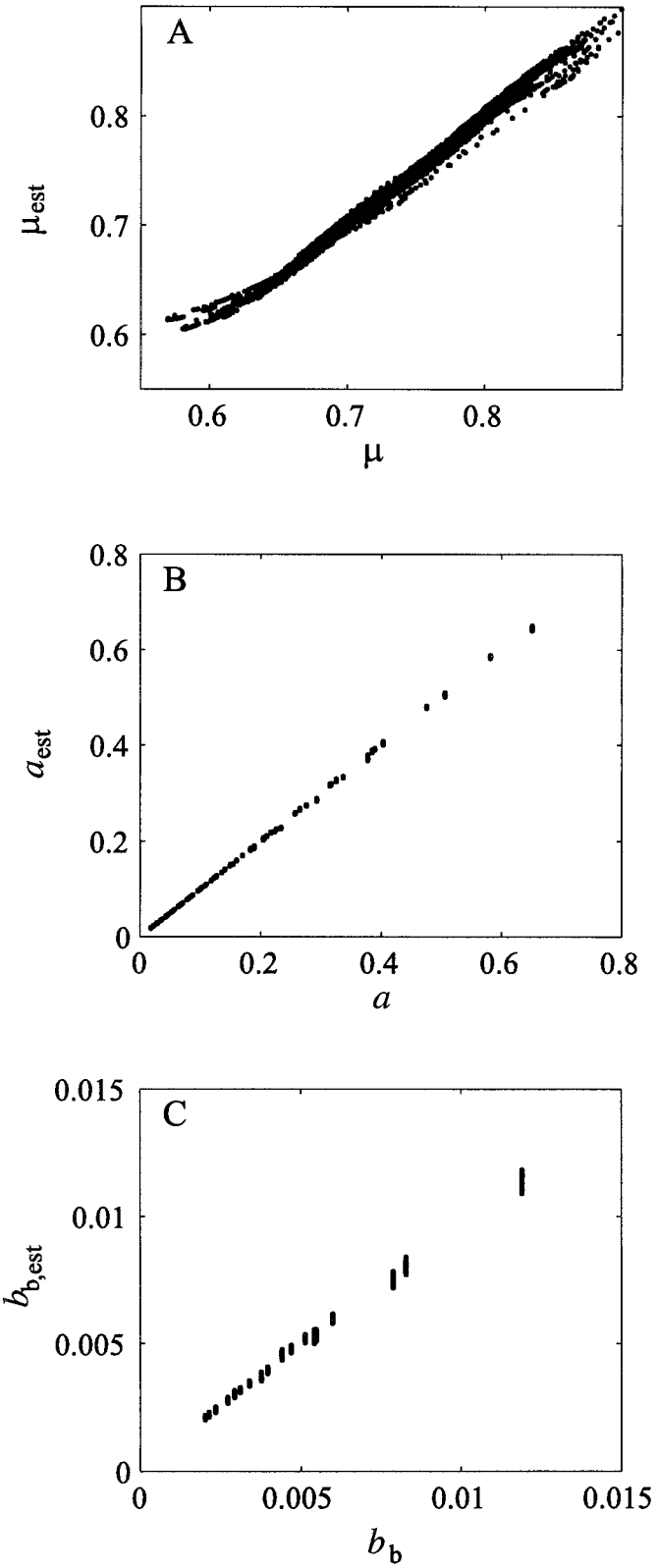

Fig. 7. (A) The relationship between the true average cosine, μ, of the light field for the 400–490 nm spectral region and its improved estimate, μ_{est2}, obtained from Eq. 10. (B) The relationship between the true absorption coefficient, a (m^{-1}), and its improved estimate, a_{est} (m^{-1}), obtained using improved estimates μ_{est2}. (C) The relationship between the true backscattering coefficient, b_b (m^{-1}), and its improved estimate $b_{b,est}$ (m^{-1}) obtained using improved estimates a_{est}. The coefficient r^2 is 0.99 for data shown in panels A, B, and C.

region did not exceed 3 nm, so no spectral adjustments were made. The MER-2048 sampled at 412, 443, and 490 nm, ac-9 at 412, 440, 488 nm, Hydroscat-6 at 442 and 488 nm, and the on-board spectrophotometric analyses of absorption provided data with high spectral resolution at 2-nm intervals. Our model retrieves the total absorption and backscattering coefficients, which can be partitioned into their additive components (e.g., Mobley 1994):

$$a(\lambda) = a_w(\lambda) + a_p(\lambda) + a_s(\lambda)$$

$$b_b(\lambda) = b_{bw}(\lambda) + b_p(\lambda) \tag{12}$$

where the subscripts w, p, and s denote pure seawater, total particulate matter, and soluble organic matter, respectively. The standard processing of Hydroscat-6 measurements yields the total backscattering coefficient $b_b(\lambda)$, which is directly comparable to the output of our model. The standard processing of ac-9 measurements provides estimates of the absorption coefficient due to the combined effect of particulate and dissolved materials. Therefore, for comparison with the model, we added the values of $a_w(\lambda)$ given in Pope and Fry (1997) to the absorption estimates from the ac-9 measurements. Similarly, we added $a_w(\lambda)$ to the sum of $a_p(\lambda)$ and $a_s(\lambda)$ estimates from on-board spectrophotometric analyses to derive the total absorption $a(\lambda)$.

The final set of data used for the comparison with the model was selected after inspecting all measurements for quality and some specific features. For example, we rejected data from the stations that showed significant differences between the downcast and upcast of the optical profiles and data from water layers with strong vertical gradients in IOPs and chlorophyll fluorescence. In addition, although measurements with MER-2048, ac-9, and Hydroscat-6 provide nearly continuous profiles with high resolution in depth, for each station we selected data only from the discrete depths within the upper 50 m layer, for which the on-board spectrophotometric analysis of water samples was made. In order to remove the noise from the measurements, the in situ IOPs were averaged over 2-m depth bins, while K_E was derived from irradiances measured in 5-m water layers.

The values of a and b_b retrieved from the measured E_d, E_u, and L_u using Eqs. 7a, 8, and 9a are compared to experimental estimates of a and b_b in Figs. 10–12. There is good agreement between the model and observation. The best fit value for the slope of the linear regression is close to 1 for the ac-9 data versus the modeled a and the Hydroscat-6 data versus modeled b_b (Figs. 11, 12). The slope value is 0.85 for the spectrophotometric data versus modeled a (Fig. 10). For the absorption coefficient, the model estimates seem to be, on average, slightly higher than the measured values by the spectrophotometric technique (Fig. 10), and slightly lower than the measured values by the ac-9 instrument (Fig. 11). If, hypothetically, the measured values were true absorptions, the standard error of the model estimates at 443 nm

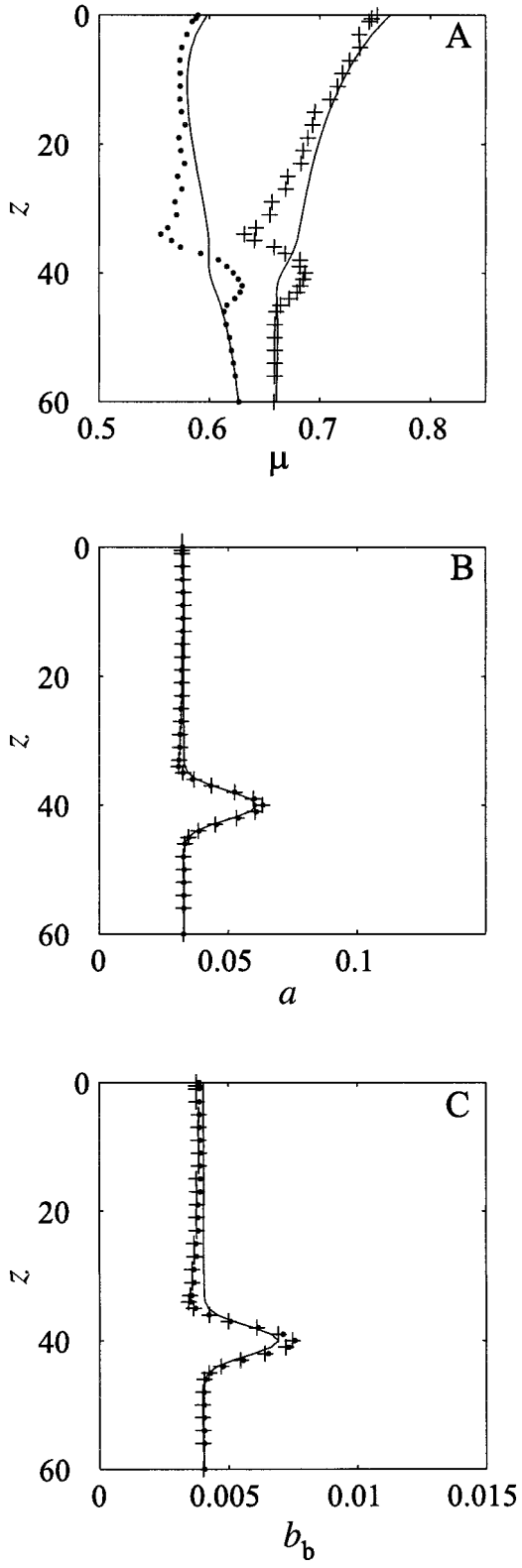

Fig. 8. Results of radiative transfer simulations for nonhomogenous ocean. (A) Comparison of the true vertical profiles of average cosine μ (solid lines) with the vertical profiles of μ estimated from our model using Eq. 10. Dots and crosses indicate values of μ estimated from radiative transfer simulations for solar zenith angle of 30 and 80°, respectively. (B) As in panel A, but the data points are for the absorption coefficient, a (m^{-1}). (C) As in panel A, but the data points are for the backscattering coefficient, b_b (m^{-1}).

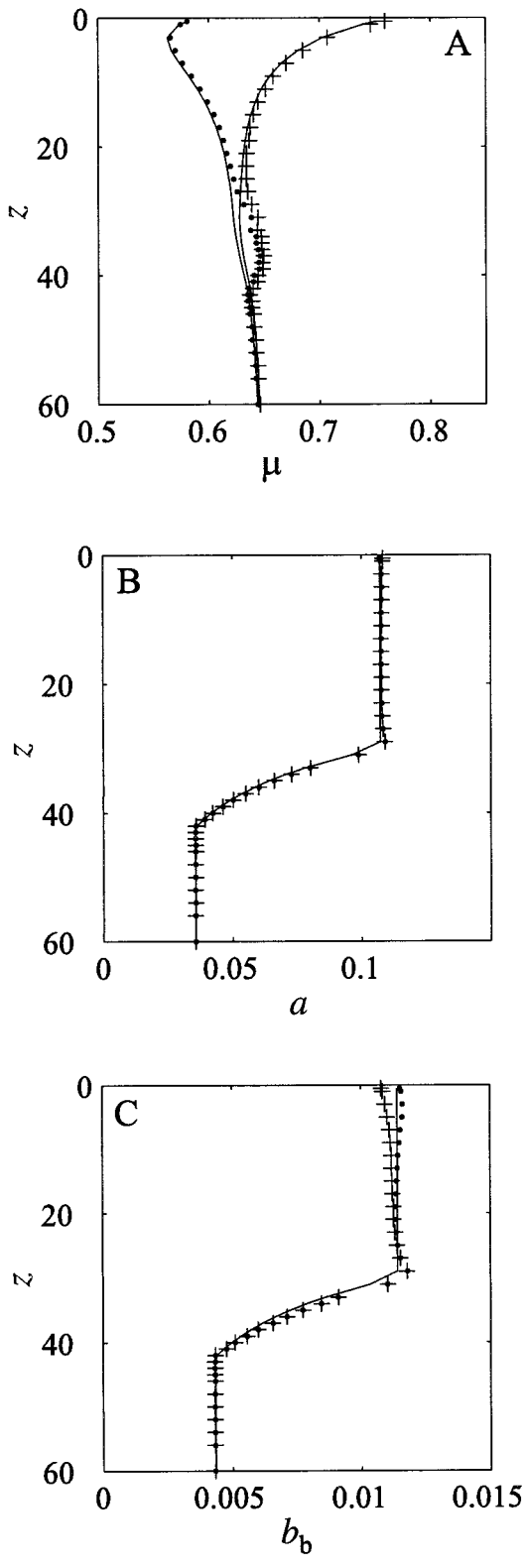

Fig. 9. As in Fig. 8, but for different vertical distributions of IOPs assumed in the model.

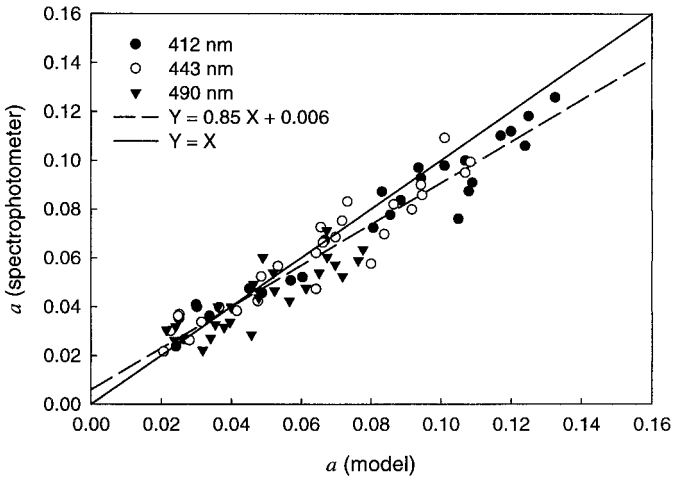

Fig. 10. Comparison of the total absorption coefficient, a (m^{-1}), estimated from spectrophotometric measurements and from our model (Eq. 8). The solid line represents perfect agreement between the observations and model. The dashed line indicates the actual regression of the observational data on model estimates ($r^2 = 0.92$). The regression equation is given where Y indicates observational data and X model estimates.

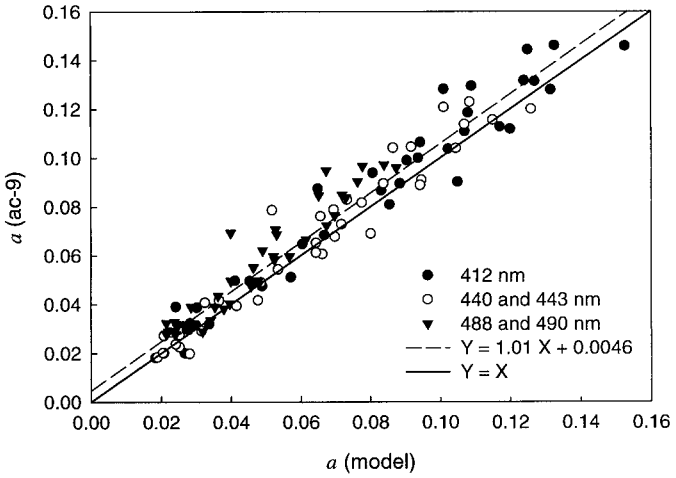

Fig. 11. As in Fig. 10, but the comparison includes the total absorption coefficient, a (m^{-1}), estimated from the ac-9 measurements ($r^2 = 0.94$).

would be 0.0085 and 0.0088 m^{-1} for the case of ac-9 and filter-pad measurements, respectively. The ε values, which provide a more balanced measure of relative error in the presence of both underestimation and overestimation (Lee et al. 1996), would be 11% and 13%, respectively. These values are similar or smaller than those obtained in recent comparisons of field observations with semi-analytic and empirical models involving inversions of the remotely sensed reflectance (Lee et al. 1996; 1998; Barnard et al. 1999).

In the case of backscattering coefficient, our model estimates tend to be higher than the Hydroscat data (Fig. 12) . It seems that some bias in the Hydroscat-6 measurements could be partly responsible for this result as the minimum observed values of b_b were as low as those for pure seawater, that is 0.0024 m^{-1} at 442 nm and 0.0015 m^{-1} at 488 nm. At the same time, the beam attenuation measurements indicated low, but measurable contribution of particles to light scattering.

The discrepancies between the model and observations are caused by the errors in the model retrieval, errors in the measurements, or both. At present it is impossible to quantify the relative importance of these sources of errors. The errors in measured values can occur for a variety of reasons. For example, the spectrophotometric analysis of particulate absorption is subject to uncertainties associated with the pathlength amplification factor and variability of the optical properties of the GF/F filters (Bricaud and Stramski 1990; Mitchell 1990). The nominal accuracy of absorption estimates from ac-9 is about 0.005 m^{-1} when careful calibration and cleaning procedures are performed (Barnard et al. 1998), which is comparable to the offset of the regression in Fig. 11. The uncertainty in the Hydroscat-6 offset (the value one would measure in the absence of any scattering) is approximately 6×10^{-4} m^{-1} at 442 nm, and the nominal accuracy of the b_b determination is about 7% (Maffione pers. comm.). Again, the offset value is close to the intercept parameter of the regression line in Fig. 12. The radiometric measurements of E_d, E_u, and L_u used as input to our model can include errors associated with the effects of sea surface waves, ship and instrument shadow, and calibration. Time and space variations in environmental variables can affect the comparison between the model and the spectrophotometric analysis of discrete water samples that were not taken simultaneously with in situ optical casts. Finally, whereas the model estimates are based on radiometric measurements representing relatively large volumes of water, the IOP measurements are made on smaller sampling volumes.

Given various sources of uncertainties in both the model estimates and measurements, the general consistency of the results shown in Figs. 10–12 is remarkable. Note also that the scatter in the data points in Figs. 10, 11 is similar to the scatter observed in Fig. 13, which compares the absorption coefficients estimated from the on-board spectrophotometric

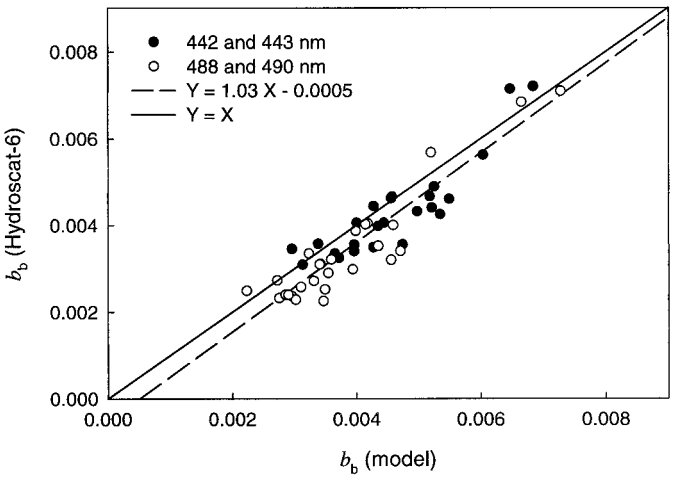

Fig. 12. As in Fig. 10 but the comparison includes the total backscattering coefficient, b_b(m^{-1}), estimated from Hydroscat-6 measurements and from our model (Eq. 9a) ($r^2 = 0.86$).

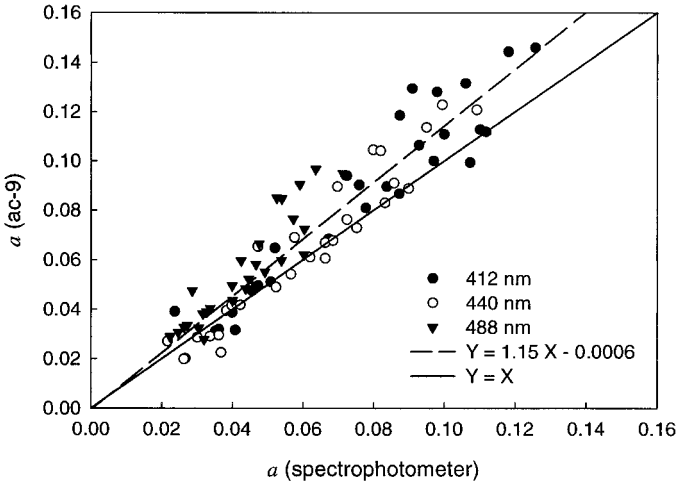

Fig. 13. Comparison of the total absorption coefficient, a (m^{-1}), from spectrophotometric measurements and ac-9 measurements. The solid line represents perfect agreement between the two estimates. The dashed line indicates the actual regression based on the plotted data points ($r^2 = 0.89$). The corresponding equation is also given with Y indicating the ac-9 data and X the spectrophotometric data.

technique and in situ ac-9 measurements. These results demonstrate that the model provides reasonable estimates of a and b_b with accuracy comparable to that of measurements.

Conclusions

By means of radiative transfer simulations we have developed a simple model to estimate a and b_b from measurements of E_d, E_u, and L_u. We have also shown that with the additional input of the beam attenuation coefficient, the estimates of a and b_b can be improved. A schematic diagram in Fig. 14 provides simple guidelines on how to utilize the model. The model allows one to readily calculate the absorption and backscattering coefficients in the blue-green spectral regions from in-water radiometric measurements, made at as few as two depths without the knowledge of surface boundary conditions and angular distribution of light. The model has been developed as a potential tool for applications to data collected from ship-based surveys and autonomous platforms such as moorings and drifters. In particular, the data sets from autonomous platforms are usually large, are limited to few depths, and lack information about the incoming radiance distribution and sea state. In addition, because such data are usually collected over prolonged periods of time when routine instrument calibration is limited, special attention has to be paid to data quality control. Our model has been developed to address these issues.

The tests of the model against the CalCoFI data from the Southern California Bight showed good agreement between the predicted and observed values of a and b_b. This agreement suggests that the model can be used to estimate a and b_b from radiometric measurements of underwater light field, to verify the quality of a and b_b values, if measured directly, and to examine the optical closure between the IOPs and AOPs. The model has been derived for a broad range of the ocean inherent optical properties that combine two distinct scenarios. In one scenario the IOPs covary with one another according to chlorophyll-based bio-optical models for case 1 waters, and in the other scenario there is no covariation among the IOPs. This implies that the model may be applicable beyond case 1 waters also. However, the model should be used with caution if significant departure from the average Petzold particle scattering phase function is expected, and further tests with field data, including coastal turbid waters, are needed.

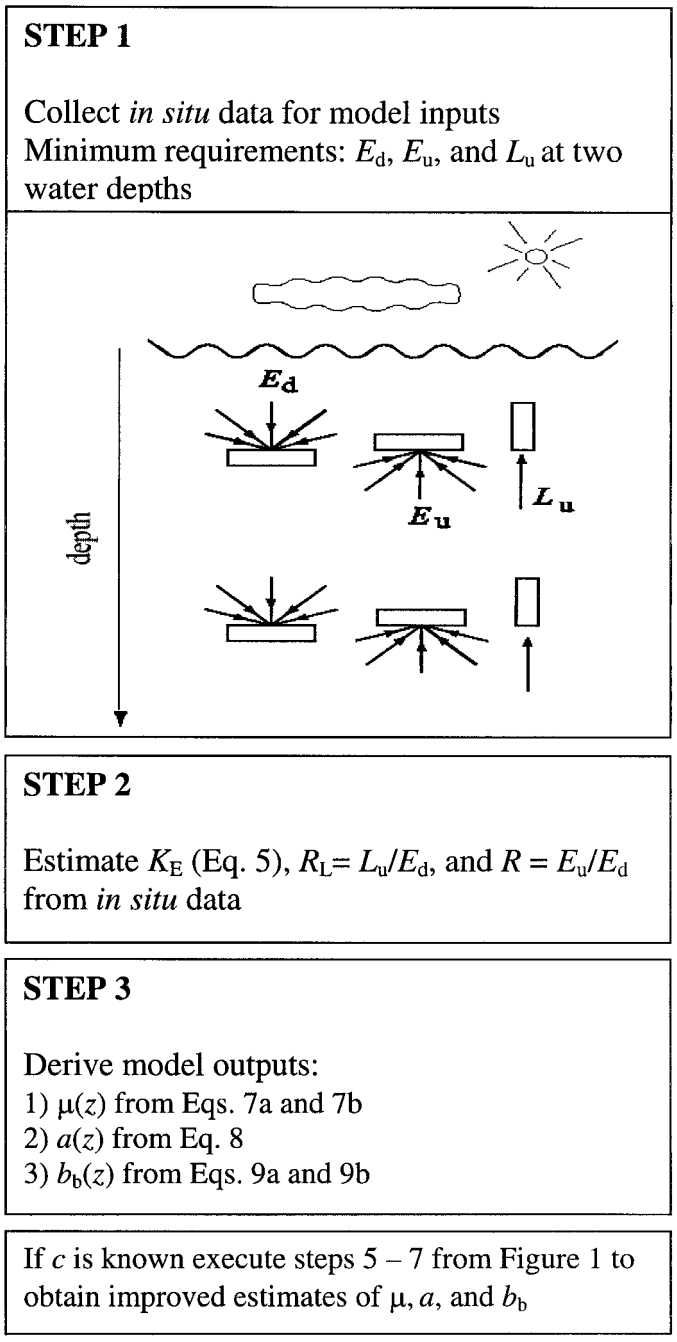

Fig. 14. Schematic diagram showing how to utilize our model.

References

BARNARD, A. H., W. S. PEGAU, AND J. R. V. ZANEVELD. 1998. Global relationships of the inherent optical properties of the oceans. J. Geophys. Res. **103:** 24955–24968.

———, J. R. V. ZANEVELD, AND W. S. PEGAU. 1999. In situ determination of the remotely sensed reflectance and the absorption coefficient: Closure and inversion. Appl. Opt. **38:** 5108–5117

BRICAUD A., A. MOREL, AND L. PRIEUR. 1981. Absorption by dissolved organic matter of the sea (Yellow substance) in the UV and visible domains. Limnol. Oceanogr. **26:** 43–53.

———, AND D. STRAMSKI. 1990. Spectral absorption coefficients of living phytoplankton and non-algal biogenous matter: A comparison between the Peru upwelling area and Sargasso Sea. Limnol. Oceanogr. **35:** 562–582.

GORDON, H. R. 1991. Absorption and scattering estimates from irradiance measurements: Monte Carlo simulations. Limnol. Oceanogr. **36:** 769–777.

———, AND G. C. BOYNTON. 1997. Radiance-irradiance inversion algorithm for estimating the absorption and backscattering coefficients of natural waters: Homogeneous waters. Appl. Opt. **36:** 2636–2641.

———, O. B. BROWN, AND M. M. JACOBS. 1975. Computed relationships between the inherent and apparent optical properties of a flat, homogenous ocean. Appl. Opt. **14:** 417–427.

———, AND A. MOREL. 1983. Remote assessment of ocean color for interpretation of satellite visible imagery—a review. Lecture notes on coastal and estuarine studies. Springer.

GREGG, W. W., AND K. L. CARDER. 1990. A simple spectral solar irradiance model for cloudless maritime atmospheres. Limnol. Oceanogr. **35:** 1657–1675.

HARRISON, A. W., AND C. A. COOMBES. 1988. An opaque cloud cover model of sky short wavelength radiance. Solar Energy **41:** 387–392.

KASTEN, F., AND G. CZEPLAK. 1980. Solar and terrestrial radiation dependent on the amount and type of cloud. Solar Energy **24:** 177–189.

KIRK, J. T. O. 1984. Dependence of relationship between inherent and apparent optical properties of water on solar altitude. Limnol. Oceanogr. **29:** 350–356.

———. 1991. Volume scattering function, average cosines, and the underwater light field. Limnol. Oceanogr. **36:** 455–467.

LEATHERS, R. A., AND N. J. MCCORMICK. 1997. Ocean inherent optical property estimation from irradiances. Appl. Opt. **36:** 8685–8698.

LEE, Z. P., K. L. CARDER, T. G. PEACOCK, C. O. DAVIS, AND J. L. MUELLER. 1996. Method to derive ocean absorption coefficients from remote-sensing reflectance. Appl. Opt. **35:** 453–462.

———, ———, R. G. STEWARD, T. G. PEACOCK, C. O. DAVIS, AND J. S. PATCH. 1998. An empirical algorithm for light absorption by ocean water based on color. J. Geophys. Res. **103:** 27967–27978.

MAFFIONE, R. A., AND D. R. DANA. 1996. Recent measurements of the spectral backward scattering coefficient in coastal waters. Ocean Optics XIII, Proc. SPIE **2963:** 154–159.

MITCHELL, B. G. 1990. Algorithm for determining the absorption coefficient of aquatic particulates using the quantitative filter technique (QFT). Ocean Optics X, Proc. SPIE **1302:** 137–148.

———, AND M. KAHRU. 1998. Algorithms for SeaWiFS developed with the CalCoFI data set. *In* CalCoFI Rep. 39, 26 pp., Calif. Coop. Oceanic Fish. Invest. Rep., La Jolla, Calif.

MOBLEY, C. D. 1994. Light and Water: Radiative transfer in natural waters. Academic.

MOORE, C., J. R. V. ZANEVELD, AND J. C. KITCHEN. 1992. Preliminary results from an in situ spectral absorption meter. Ocean Optics XI, Proc. SPIE **1750:** 330–337.

MOREL, A. 1974. Optical properties of pure water and pure seawater, p. 1–24. *In* N.G. Jerlov, and Steeman Nielsen [eds.]. Optical aspects of oceanography, Academic.

———. 1988. Optical modeling of the upper ocean in relation to its biogenous matter content (case 1 waters). J. Geophys. Res. **93:** 10749–10768.

———. 1991. Light and marine photosynthesis: A spectral model with geochemical and climatological implications. Prog. Oceanogr. **26:** 263–306.

———, AND B. GENTILI. 1991. Diffuse reflectance of oceanic waters: Its dependence on sun angle as influenced by the molecular scattering contribution. Appl. Opt. **30:** 4427–4438.

———, AND ———. 1993. Diffuse reflectance of oceanic waters. II, bidirectional aspects. Appl. Opt. **32:** 6864–6879.

———, AND L. PRIEUR. 1977. Analysis of variations in ocean color. Limnol. Oceanogr. **22:** 709–722.

MUELLER J. L., AND R. W. AUSTIN. 1992. Ocean Optics Protocols for SeaWiFS validation, SeaWiFS Technical Report Series, NASA Tech. Memo. 104566, vol. 25.

PETZOLD, T. J. 1972. Volume scattering functions for selected ocean waters. Scripps Inst. Oceanogr. Ref. 72–78.

POPE, R. M., AND E. S. FRY. 1997. Absorption spectrum (380–700 nm) of pure water: II. Integrating cavity measurements. Appl. Opt. **36:** 8710–8723.

STAVN, R. H. 1993. Effects of Raman scattering across the visible spectrum in clear ocean water: A Monte Carlo study. Appl. Opt. **32:** 6853–6863.

STRAMSKA M., AND D. FRYE. 1997. Dependence of apparent optical properties on solar altitude: Experimental results based on mooring data collected in the Sargasso Sea. J. Geophys. Res. **102:** 679–691.

TIMOFEEVA, V. A. 1979. Determination of light-field parameters in the depth regime from irradiance measurements. Iz. Atmos. Ocean. Phys. **15:** 774–776. Engl. trans.

ZANEVELD, J. R. V., R. BARTZ, AND J. C. KITCHEN. 1990. Reflective-tube absorption meter. Ocean Optics X, Proc. SPIE **1302:** 124–136.

Received: 21 June 1999
Accepted: 17 December 1999
Amended: 17 January 2000